

Shear melting and recovery of crosslinkable cellulose nanocrystal-polymer gels

Abhinav Rao^a, Thibaut Divoux^{b, c}, Gareth H. McKinley^a, and A. John Hart^a

^a*Department of Mechanical Engineering, Massachusetts Institute of Technology, Cambridge MA 02139, USA*

^b*Centre de Recherche Paul Pascal, CNRS UMR 5031 - 115 avenue Schweitzer, 33600 Pessac, France*

^c*MultiScale Material Science for Energy and Environment, UMI 3466 CNRS-MIT, 77 Massachusetts Avenue, Cambridge, Massachusetts 02139, USA*

1 CNC Size Distribution

Dynamic light scattering (DLS) measurements were performed on 8.5% wt. CNC composite gels after the CNCs were dispersed by sonication. The weight fraction is selected to ensure that the gels flow easily for insertion into the cuvettes for DLS measurements. The measurements were performed with a DynaPro Nanostar instrument. The aggregates in the freeze-dried CNC powder are dispersed into nanoparticles, with a majority of the particles having a width of about 2.5 nm. This corresponds to the size of individual CNCs from previous observations of CNCs extracted from wood fibers.¹ Fig. S1 shows the DLS intensity distribution of the CNCs measured after probe sonication. The numerical description of the DLS peaks, including the mass distributions are provided in Table S1. The length of the CNCs was observed using atomic force microscopy (AFM) of a dried CNC film, as shown in the topography image in Fig. S2. The length of the CNCs is around 100 nm, similar to previous observations on CNCs extracted by acid hydrolysis from wood fibers.² Here, the AFM tip diameter with 7 nm does not capture individual CNCs, rather the widths observed are small aggregates formed during the drying process.

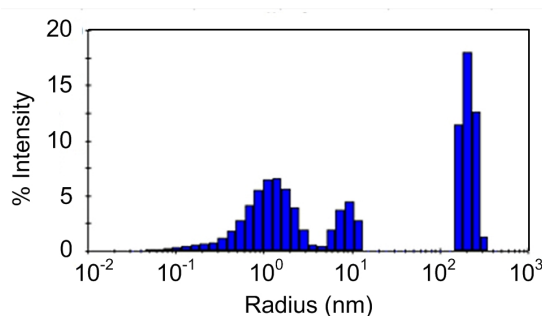


Figure S1: Size distribution of CNCs in an 8.5% wt. composite gel after probe sonication measured using DLS.

Item	Radius (nm)	PD %	M_w (kDa)	Mass %
Peak 1	1.271	63.8	6	99.9
Peak 2	8.933	22.8	565	0.1
Peak 3	216.6	19.7	982087	0

Table S1: Size distribution of CNCs after probe sonication measured using DLS.

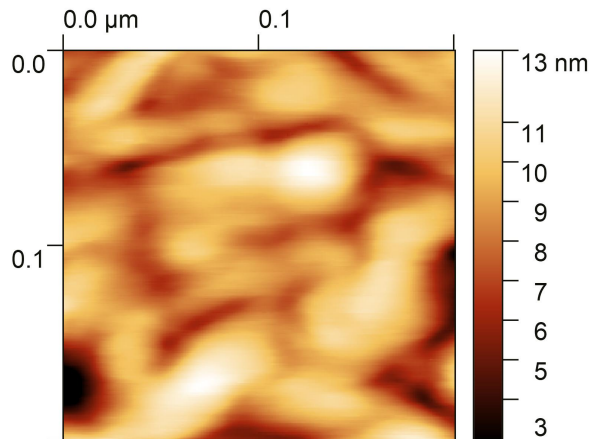


Figure S2: Atomic force microscopy of CNCs showing their rod-like structure.

2 Effect of crosslinkers

The composite CNC gels (CG) contain only the epoxide oligomer and solvent, while the UV-curable CNC gels (UV-CG) contain in addition a cationic photoinitiator and a polyamine thermal crosslinker. To examine whether the inclusion of the crosslinkers alters the physical interaction between the CNCs, or result in a chemical reaction, we compare the FTIR spectra of the two types of gels, prior to the application of any significant shear history. The composite CNC gel and the UV-curable CNC gel have 12.5% wt. and 12% wt. CNCs respectively (Fig. S3a and S3b). The key peaks of interest in these two spectra are identical. These include the broad hydroxyl (OH) peak between $3200\text{-}3600\text{ cm}^{-1}$, the CH peak around 2950 cm^{-1} , the COC bond due to the pyranose ring on cellulose at 1100 cm^{-1} and the C=O peak from DMF located between $1600\text{ and }1700\text{ cm}^{-1}$. Therefore, we conclude that the crosslinkers do not have any discernable chemical effect on the gels. The electrostatic repulsion between the CNCs is dependent on the Debye screening length of the medium.³ The presence of the thermal crosslinker and cationic photoinitiator modifies the nominal Debye screening length resulting in the inhibition of electrostatic repulsion between the CNCs. This allows the formation of clusters of CNC particles governed by van der Waals attraction in the UV-curable gels.

3 Structural characterization

Small-angle X-ray scattering (SAXS) measurements were performed on composite gels with CNC mass fractions of 8.5%, 10.5% and 12.5%, using a SAXSLab system with a Dectris Pilatus 300K

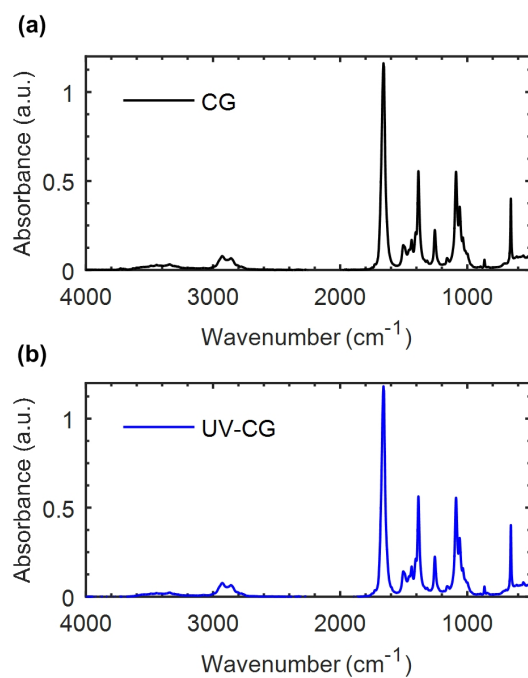


Figure S3: FTIR spectra of two types of CNC gels: (a) a composite gel (CG) with 12.5% wt. CNCs, and (b) a UV curable gel (UV-CG) with 12% wt. CNCs. The spectra for each sample are indistinguishable.

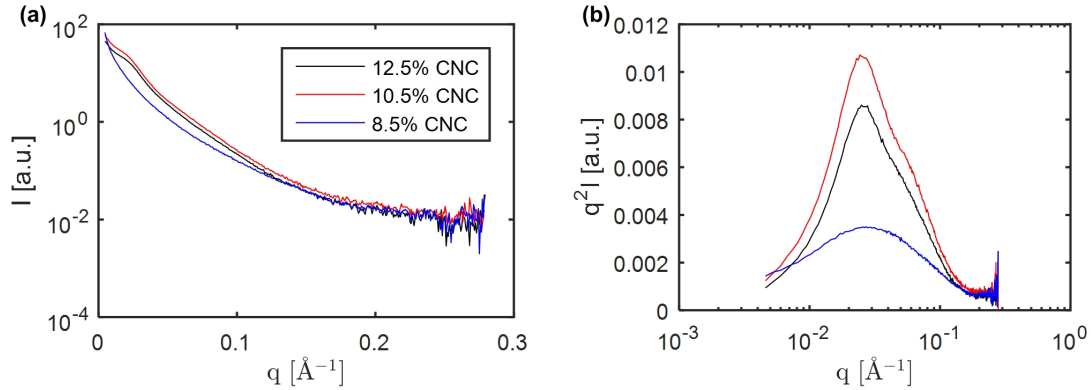


Figure S4: Small-angle X-ray scattering measurements of composite gels with CNC mass fractions of 8.5%, 10.5% and 12.5%: (a) Azimuthally averaged intensity, I versus wavevector q and (b) Kratky plot representation of the scattering intensity showing $q^2 I$ versus q .

detector. The gels were loaded into cells with Mylar windows, sealed with rubber o-rings to prevent solvent evaporation. The azimuthal average scattering intensity versus the scattering vector for the composite gels is shown in Fig. S4a. A Kratky plot showing $q^2 I$ versus q is shown in Fig. S4b is a useful representation as this data, as a pronounced peak in the low q region is characteristic of kinetically arrested inhomogeneities in polymer gels.⁴ In aqueous CNC suspensions, the peak in the Kratky plot is indicative of locally aligned clusters of CNCs, and can be correlated to the chiral nematic pitch in liquid crystalline domains.⁵ Here, the composite gels without crosslinkers are expected to have a greater degree of local CNC alignment, driven by the repulsive charges. In the UV-curable gels, the charge screening due to the presence of the crosslinkers also hinders the alignment of CNCs into tightly packed domains. This distinction between the two types of gels is also manifested in the observed color of the gels as seen in Fig. 1.

4 Further details comparing viscoelastic recovery of the composite and the UV-curable gels

The elastic properties of composite gels do not show the same recovery as seen in the UV-curable gels. During each recovery period, G' shows a weak aging with time, with a relatively small change. Fig. S5 shows the recovery of the elastic modulus of a 12.5% wt. composite gel (CG) with and a 12% wt. UV-curable gel (UV-CG) after the application of a shear strain of $\gamma_T = 7 \cdot 10^3$. The 12% wt. UV-curable gel exhibits an initial elastic modulus $G' = 22$ Pa, which recovers to about $G' = 300$ Pa after 360 s. By contrast, for the same accumulated strain, a 12.5% wt. composite gel exhibits an initial elastic modulus $G' = 818$ Pa, which increases to $G' = 930$ Pa after 360 s. In the case of the composite gel, the presence of repulsive interactions in addition to attractive hydrogen bonds results in “caging” of colloidal particles, which is responsible for the slow dynamics of recovery described above.

Fig. S6 shows the evolution of the viscous modulus G'' with time for the recovery of a 11% wt. UV curable gel as a complement to the evolution of G' shown in Fig. 4a in the main text. A

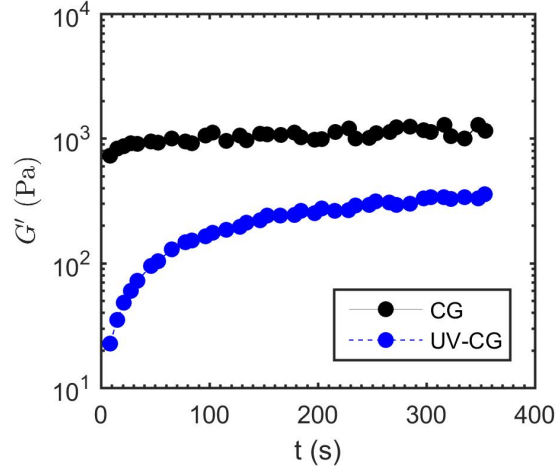


Figure S5: Comparison of the recovery of the elastic modulus of a 12.5% wt. composite gel and a 12% wt. UV-curable gel. The evolution of G' for both types of gels were recorded after the application of a cumulative strain of $\gamma_T = 7 \cdot 10^3$.

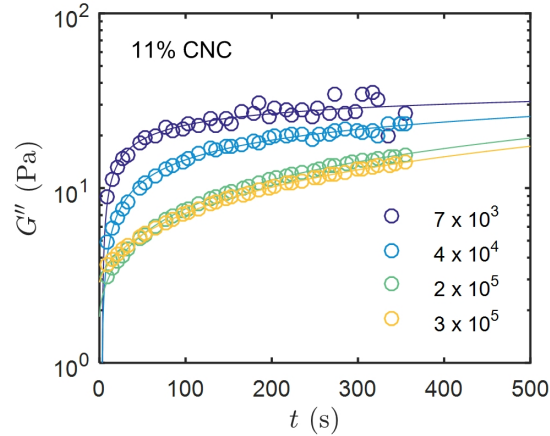


Figure S6: Recovery of the viscous modulus G'' versus time after shear-melting steps for a UV-curable gel with 12% wt. CNC. The cumulative strain experienced by the sample before each recovery is indicated on the graph. The fits corresponds to the best power-law fit of the data described by Eq. 2 in the main text, in which G' is replaced by G'' .

power-law function identical to Eq. 2 describes the evolution of G'' during the recovery.

The evolution of G' versus time during the recovery of composite gels, without crosslinkers, following the cessation of a shear-melting step is shown in Fig. S7 for gels with different CNC concentrations. For a detailed description of the rheology protocol, refer to Fig. 3 in the main text. In the absence of crosslinkers, the repulsive electrostatic interactions between the CNC particles prevent the formation of percolating CNC clusters. For 8.5% wt. composite gels, a small strain ($\gamma_T = 3 \cdot 10^3$) is sufficient to fully and irreversibly fluidize the gel. The same finding applies to the

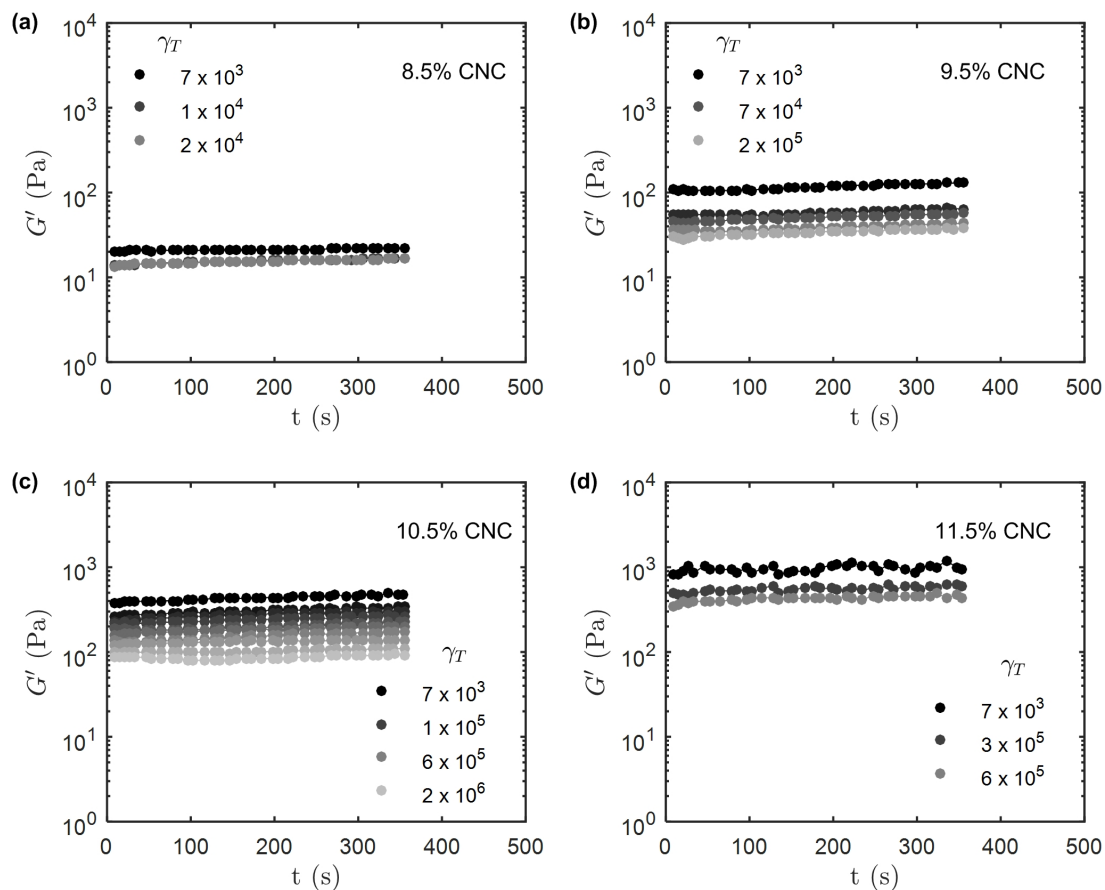


Figure S7: Absence of time-dependence in the recovery of composite gels at different cumulative strains, after successive shear-melting steps indicated by increasing values of γ_T for (a) 8.5%, (b) 9.5%, (c) 10.5% and (d) 11.5% wt. CNC gels. The viscoelastic recovery was monitored by applying small amplitude oscillatory shear (stress amplitude $\sigma_0 = 0.5$ Pa and frequency $f = 1$ Hz) following the same protocol as the one used for the UV curable gels (see main text Fig. 4). To aid the quantitative comparison with Fig. 4 in the main text, the vertical scale of each graph is set to match that used for the UV curable gels.

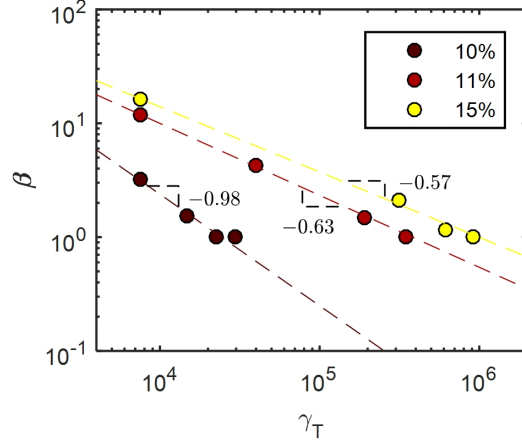


Figure S8: Dimensionless rescaling factor β vs the cumulative strain γ_T for UV-curable gels of three different concentrations: 10% wt., 11% wt. and 15% wt. (The corresponding rescaled curves are reported in Fig. 4(b)–(d) in the main text.) The dashed lines correspond to the best power-law fit of the data: $\beta = k\gamma_T^\zeta$. The exponent ζ is reported on the graph.

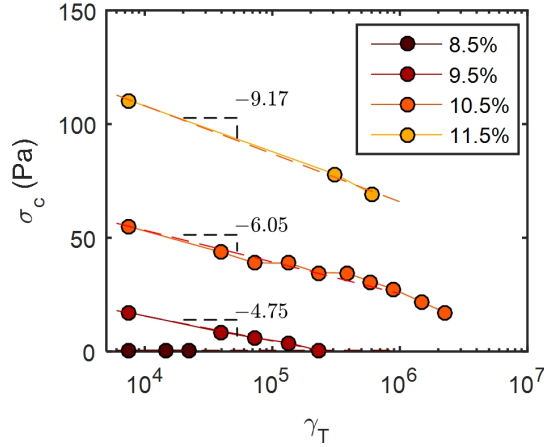


Figure S9: Yield stress σ_c of composite gels for different CNC concentrations ranging between 8.5% wt. and 15% wt. vs the cumulative strain γ_T . Each yield stress was determined by performing a stress sweep at a frequency of $f = 1$ Hz. The dashed lines correspond to the best fit of the data with a logarithmic function: $\sigma_c = \sigma_c^{(0)} + B \ln(\gamma_T)$, where $\sigma_c^{(0)}$ and B serve as free parameters. The fit parameter B is reported on the graph.

9.5% wt. CNC gel, which is irreversibly fluidized at $\gamma_T = 2 \cdot 10^5$. At higher concentrations of CNCs, (i.e. 10.5% wt. and 11.5% wt.), the elastic modulus progressively decreases with increasing strain, but the gel maintains a finite yield stress for strains of at least $\gamma_T = 6 \cdot 10^5$.

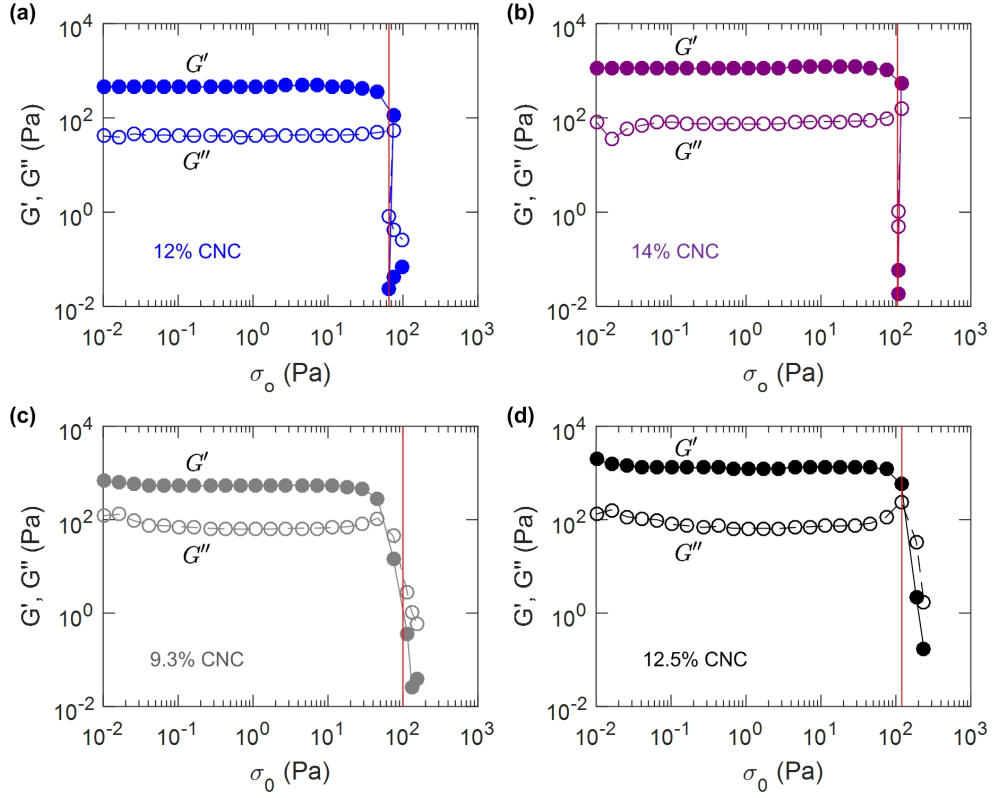


Figure S10: Stress sweeps on polymer-CNC gels showing G' (filled symbols) and G'' (open symbols) versus the stress amplitude, σ_0 . (a) 12% wt. and (b) 14% wt. UV-curable CNC gels. (c) 9.3% wt. and (d) 12.5% wt. composite CNC gel. Stress sweeps are performed at $f = 1$ Hz following a 60 s pre-shear at $\dot{\gamma} = 500 \text{ s}^{-1}$ and a recovery period of 1000 s. The vertical red lines indicate the stresses used for the creep experiments described in Fig. 9a and Fig. 10a of the main text.

5 Rescaling factors

The factor β used to rescale the time axis of $G'(t)$ and $G''(t)$ for the 10% wt., 11% wt. and 15% wt. UV-curable gels that are presented in Fig. 4b–4d are reported in Fig. S8 as a function of the cumulative strain γ_T . For each UV-curable gel, the rescaling factor β follows a power-law with respect to γ_T . The power-law exponent decreases for increasing CNC concentrations: from about $\zeta = -0.97$ for the 10% wt. gel to $\zeta = -0.57$ for the 15% wt. gel.

6 Comparison between the yielding behavior of composite gels and UV-curable gels

The yield stress determined after each recovery period is shown in Fig. S9. As seen in the case of the UV-curable gels, each cycle of shear flow results in a permanent reduction in the number of hydrogen bonds. Thus, the composite gels show a lower yield stress with each cycle of shear melting and recovery, as the cumulative strain applied on the gels increases.

The applied shear stress magnitude for the creep experiments described in Fig. 9 and Fig. 10 were chosen in the vicinity of the yield stress, σ_c of the sample at the present age. The latter value was determined by performing stress sweeps at $f = 1$ Hz. The stress sweeps are reported in Fig. S10a and S10b for the 12% wt. and 14% wt. UV-curable gels, and in Fig. S10c and S10d for the 9.3% wt. and 12.5% wt. composite gels. The vertical red lines indicate the stress at which the subsequent creep experiments were performed. During the stress sweep, the UV-curable gels show an abrupt yielding transition as both G' and G'' drop by about two orders of magnitude within around 20 Pa of stress amplitude. By comparison, the yielding of the composite gels in the absence of charge screening crosslinkers, is observed to be more gradual. Around the yield stress, the elastic and viscous modulus show a smooth decay over about a decade of over a range of around 100 Pa in stress amplitude. The abrupt yielding of the UV-curable gels is reminiscent of a brittle-like failure scenario, whereas the progressive failure of the composite gels is more ductile-like. The study of large deformations of biopolymer gels with different intermolecular interactions shows that after yielding, the elastic modulus “weak” gels displays a significantly higher sensitivity to applied deformation, in comparison with “strong” gels.⁶ In the case of the composite gels the absence of charge screening enables repulsive interactions and provides an additional entrapment effect for the CNCs, effectively resulting in a stronger gel.

References

- [1] J. P. F. Lagerwall, C. Schütz, M. Salajkova, J. Noh, J. Hyun Park, G. Scalia and L. Bergström, *NPG Asia Materials*, 2014, **6**, e80–e80.
- [2] R. R. Lahiji, X. Xu, R. Reifenger, A. Raman, A. Rudie and R. J. Moon, *Langmuir*, 2010, **26**, 4480–4488.
- [3] A. M. Smith, A. A. Lee and S. Perkin, *The Journal of Physical Chemistry Letters*, 2016, **7**, 2157–2163.
- [4] E. M. Saffer, M. A. Lackey, D. M. Griffin, S. Kishore, G. N. Tew and S. R. Bhatia, *Soft Matter*, 2014, **10**, 1905.

- [5] C. Schütz, M. Agthe, A. B. Fall, K. Gordeyeva, V. Guccini, M. Salajková, T. S. Plivelic, J. P. F. Lagerwall, G. Salazar-Alvarez and L. Bergström, *Langmuir*, 2015, **31**, 6507–6513.
- [6] D. R. Picout and S. B. Ross-Murphy, *The Scientific World Journal*, 2003, **3**, 105–121.